Received: 8 July 2021 | Revised: 1 February 2022 | Accepted: 13 March 2022

DOI: 10.1002/mp.15625

RESEARCH ARTICLE

MEDICAL PHYSICS

Experimental validation of 4D log file-based proton dose reconstruction for interplay assessment considering amplitude-sorted 4DCTs

Saskia Spautz[1] | **Annika Jakobi**[1,2,3] | **Arturs Meijers**[4] | **Nils Peters**[1,2] | **Steffen Löck**[1,3,5] | **Antje-Christin Knopf**[4,6] | **Esther G.C. Troost**[1,2,3,5,7] | **Christian Richter**[1,2,3,5] | **Kristin Stützer**[1,2]

[1]OncoRay—National Center for Radiation Research in Oncology, Faculty of Medicine and University Hospital Carl Gustav Carus, Technische Universität Dresden, Helmholtz-Zentrum Dresden—Rossendorf, Dresden, Germany

[2]Helmholtz-Zentrum Dresden—Rossendorf, Institute of Radiooncology—OncoRay, Dresden, Germany

[3]Department of Radiotherapy and Radiation Oncology, Faculty of Medicine and University Hospital Carl Gustav Carus, Technische Universität Dresden, Dresden, Germany

[4]Department of Radiation Oncology, University Medical Center Groningen, University of Groningen, Groningen, The Netherlands

[5]German Cancer Consortium (DKTK), Partner Site Dresden, German Cancer Research Center (DKFZ), Heidelberg, Germany

[6]Department 1 of Internal Medicine, Center for Integrated Oncology Cologne, University Hospital of Cologne, Cologne, Germany

[7]National Center for Tumor Diseases (NCT), Partner Site Dresden, Germany: German Cancer Research Center (DKFZ), Heidelberg, Germany; Faculty of Medicine and University Hospital Carl Gustav Carus, Technische Universität Dresden, Dresden, Germany, and; Helmholtz Association / Helmholtz-Zentrum Dresden - Rossendorf (HZDR), Dresden, Germany

Correspondence
Kristin Stützer, OncoRay—National Center for Radiation Research in Oncology, Medizinische Fakultät Carl Gustav Carus, TU Dresden, Fetscherstraße 74, 01307 Dresden, Germany.
Email: kristin.stuetzer@oncoray.de

Abstract

Purpose: The unpredictable interplay between dynamic proton therapy delivery and target motion in the thorax can lead to severe dose distortions. A fraction-wise four-dimensional (4D) dose reconstruction workflow allows for the assessment of the applied dose after patient treatment while considering the actual beam delivery sequence extracted from machine log files, the recorded breathing pattern and the geometric information from a 4D computed tomography scan (4DCT). Such an algorithm capable of accounting for amplitude-sorted 4DCTs was implemented and its accuracy as well as its sensitivity to input parameter variations was experimentally evaluated.

Methods: An anthropomorphic thorax phantom with a movable insert containing a target surrogate and a radiochromic film was irradiated with a monoenergetic field for various 1D target motion forms (sin, sin^4) and peak-to-peak amplitudes (5/10/15/20/30 mm). The measured characteristic film dose distributions were compared to the respective sections in the 4D reconstructed doses using a 2D γ-analysis (3 mm, 3%); γ-pass rates were derived for different dose grid resolutions (1 mm/3 mm) and deformable image registrations (DIR, automatic/manual) applied during the 4D dose reconstruction process. In an additional analysis, the sensitivity of reconstructed dose distributions against potential asynchronous timing of the motion and machine log files was investigated for both a monoenergetic field and more realistic 4D robustly optimized fields

by artificially introduced offsets of ±1/5/25/50/250 ms. The resulting dose distributions with asynchronized log files were compared to those with synchronized log files by means of a 3D γ-analysis (1 mm, 1%) and the evaluation of absolute dose differences.

Results: The induced characteristic interplay patterns on the films were well reproduced by the 4D dose reconstruction with 2D γ-pass rates ≥95% for almost all cases with motion magnitudes ≤15 mm. In general, the 2D γ-pass rates showed a significant decrease for larger motion amplitudes and increase when using a finer dose grid resolution but were not affected by the choice of motion form (sin, sin^4). There was also a trend, though not statistically significant, toward the manually defined DIR for better quality of the reconstructed dose distributions in the area imaged by the film. The 4D dose reconstruction results for the monoenergetic as well as the 4D robustly optimized fields were robust against small asynchronies between motion and machine log files of up to 5 ms, which is in the order of potential network latencies.

Conclusions: We have implemented a 4D log file-based proton dose reconstruction that accounts for amplitude-sorted 4DCTs. Its accuracy was proven to be clinically acceptable for target motion magnitudes of up to 15 mm. Particular attention should be paid to the synchronization of the log file generating systems as the reconstructed dose distribution may vary with log file asynchronies larger than those caused by realistic network delays.

KEYWORDS
4D dose, interplay effect, log file-based dose reconstruction, pencil beam scanning, proton therapy

1 | INTRODUCTION

Pencil beam scanning (PBS) allows for highly conformal proton beam therapy and has been established as the major modality of proton beam application. When treating targets undergoing breathing-induced motion, the interference of the dynamic beam delivery and the motion of the tumor can lead to serious dose distortions. This so-called interplay effect has been investigated in numerous studies showing that its impact depends on various factors, such as the motion magnitude and direction, the number of treatment fractions, and the beam scanning parameters like spot size, spot spacing, scanning speed, and scanning direction.[1–4] The steep density gradients in the thoracic region can further increase dose deviations as they may also vary with breathing and strongly impact the proton range.[5,6]

A mitigation of motion-induced effects can be achieved by different approaches such as rescanning,[7–10] gating,[8–12] four-dimensional (4D) robust treatment planning,[13,14] or abdominal compression.[15,16] However, depending on the patient, such techniques might not completely mitigate interplay effects and their resulting dose distortions. While pre-treatment interplay analyses[17–19] provide valuable insights into motion-related robustness at the stage of plan approval, they are not suited to consider the influence of the actual interfractional changes in patient anatomy and breathing pattern.[20–22] Monitoring the applied dose distribution with regard to interplay effects during the entire treatment course can be employed to check whether clinical goals, for example target coverage or normal tissue sparing are fulfilled. By using the treatment machine log files, containing temporal and spatially resolved information of the dynamic PBS beam delivery, in combination with the synchronized log files of a motion monitoring device as a surrogate for the target motion during irradiation, the fraction dose can be calculated retrospectively for the patient geometry depicted in a 4D computed tomography scan (4DCT). The 4D interplay-affected dose is reconstructed by assigning each PBS spot of the plan to the corresponding 4DCT phase and accumulating the subplan doses per computed tomography (CT) phase via deformation vector fields. Different in-house solutions for such a 4D dynamic dose reconstruction workflow have been presented.[23–26]

Meijers et al.[27] introduced the first clinically applied 4D proton dose reconstruction algorithm that is capable of using combined datasets of motion log files acquired during patient treatment, PBS treatment log files, and patient 4DCT images. To yield accurate results, the PBS spot assignment to the different CT breathing phases needs to be consistent with the 4DCT reconstruction method. The algorithm by Meijers et al. was designed for a PBS spot sorting that considers a phase-based 4DCT image reconstruction. The raw data for the respective 3DCT images are thus equally distributed over time within a breathing cycle without considering the actual breathing curve amplitudes. At the University Proton Therapy Dresden (UPTD), 4DCTs are

reconstructed based on relative amplitude sorting of the raw data, which has the advantage of a better image artifact reduction[28,29] as it compensates for differences in the breathing signal shape such as changing ratios of inhalation–exhalation duration over different breathing cycles. Consequently, to perform the 4D log file-based dose reconstruction for patients treated at UPTD, the PBS spot assignment to the CT phases needs to be compatible with the amplitude-based 4DCT reconstruction.

In this study, we investigated the in-house 4D log file-based dose reconstruction introduced by Meijers et al.[27] after adapting the algorithm to fit a relative amplitude-based 4DCT reconstruction. The aim of our experimental phantom study was twofold: (1) we assessed the validity of the 4D log file-based reconstruction results by comparing them to reference dose visualizations on radiochromic films. To detect potential deficiencies and limitations of the algorithm, we induced distinct interplay-affected dose distributions in a patient-like phantom geometry with regular motion. These include clinically relevant but also extreme magnitudes to investigate up to which target motions accurate dose reconstruction results can be expected. We further quantified how improvements in the applied deformable image registration and the dose grid resolution influenced the results. (2) We quantified the sensitivity of the dose reconstruction against temporal asynchronies of various magnitudes between the machine log files and the motion log files (recorded by a pressure belt system). As the impact of an asynchrony between the two log file systems and spot delivery timing might be interdependent, additional calculations were performed for more clinical-like plans, that is aiming for a homogeneous dose distribution to the target and thus using various, mainly lower spot doses and a faster delivery per spot.

2 | MATERIAL AND METHODS

2.1 | 4D log file-based dose reconstruction algorithm considering amplitude-sorted 4DCTs

To calculate the interplay-affected delivered dose, a 4D log file-based reconstruction algorithm was adapted from Meijers et al.[27] Each delivered spot is assigned to a certain CT phase according to its delivery time (taken from the machine log file) and the corresponding motion status (taken from the motion log file). By doing so, a subplan is generated for each 4DCT phase. While the original algorithm performs a straightforward spot assignment in accordance to a phase-based reconstructed 4DCT by considering equal time intervals per CT phase within each breathing cycle, our adjusted algorithm accounts for the more complex timing of the relative amplitude-based reconstructed 4DCT phases (Figure S1).

The 4D dose reconstruction starts with the initial motion log file post-processing. A potential clock offset for the motion monitoring device observed by the network time protocol can be corrected by shifting the time axis accordingly. After smoothing (Savitzky-Golay-filter) the breathing curve signal, the local points of maximal inhalation and exhalation are identified in the cropped signal matching with the delivery timeframe of the treatment field. As patient breathing curves can show relevant fluctuations, such as additional local extrema and amplitude drifts between breathing cycles, the algorithm is guided by a user-specified amplitude that separates the inhalation and exhalation extrema, that is only one inhalation maximum and minimum per breathing cycle are identified above and below this threshold, respectively. If necessary, the user can add, delete, and adjust the identified extrema manually before proceeding with the automatic spot assignment.

According to the relative amplitude-based 4DCT reconstruction, the motion signal between two consecutive extrema is locally scaled to relative amplitudes (0 to 1 for the ascending slopes of inspiration and 1 to 0 for the descending slopes of expiration). Within each breathing cycle, the algorithm interpolates the time points t_i that match with the trigger amplitudes a_i on the ascending or descending edge used for reconstructing the respective inhalation or exhalation CT phases. The inhale/exhale amplitude a_i of the ith CT phase is automatically retrieved from the CT naming in the treatment planning system (TPS) extracted from the respective DICOM information. Spots delivered after such a trigger time point t_i and before the subsequent t_{i+1} are assigned with their log file-recorded positions and MUs to the subplan for the ith CT phase. In the case that the difference between subsequent trigger times ($\Delta t_i = t_{i+1} - t_i$) is larger than the raw data bins used for CT reconstruction ($T_{raw} = 250$ ms), spots delivered in the interval $[t_i + T_{raw}, t_{i+1}]$ are equally split among the respective subplans. In other words, spots delivered after $t_i + 0.5(T_{raw} + \Delta t_i)$ are assigned to the subplan of the next CT phase ($i + 1$). The created subplans (in DICOM RT format) are imported into the TPS and subplan doses are calculated on the corresponding CT phases, deformed via the deformable image registrations (DIR) to the reference CT phase and accumulated to acquire the interplay-affected dose distribution.

2.2 | Phantom study for validation of the algorithm

2.2.1 | Experimental setup

A dynamic thorax phantom (CIRS, Norfolk, VA, USA) with a moveable rod located in the left lung (Figure 1a)

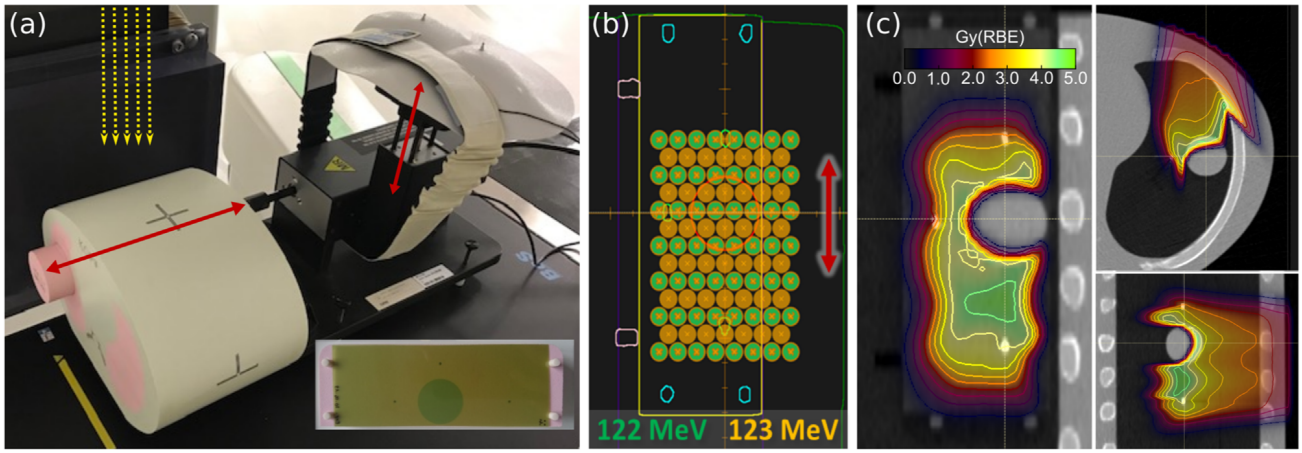

FIGURE 1 (a) Dynamic thorax phantom including an insert with a 3 cm spherical tumor model and the radiochromic film, shown in detail in the bottom right, and the pressure belt for motion acquisition wrapped around the chest plate attached to the motion surrogate platform. Red arrows indicate the motion directions of the insert and surrogate, and the dashed yellow arrows the incident beam direction of an anterior field, respectively, (b) spot positions of the quasi-monoenergetic field for the 30 mm peak-to-peak tumor motion shown with contours of the coronal isocenter slice in the maximum exhalation phase (most cranial target position), and (c) the orthogonal isocenter slices of the corresponding static dose distribution (which was not generated with the intention to cover the tumor insert itself as described in the text). The coronal plane corresponds to the expected static dose distribution on the radiochromic film

was aligned by means of orthogonal X-ray imaging at the isocenter in the clinical treatment room of the UPTD. The moveable rod contained an insert with a spherical soft-tissue tumor model of 3 cm diameter and three radiopaque markers in the coronal isocenter plane. A EBT3 Gafchromic film cutting (Ashland, Covington, KY, USA; LOT11041303) was positioned between the two halves of the insert at the coronal isocenter plane, intersecting the tumor model. The rod performed a 1D sinusoidal or a sin^4 motion in cranio-caudal direction with a constant cycle time of 5 s and a peak-to-peak amplitude of either 5 mm, 10 mm, 15 mm, 20 mm or 30 mm, respectively. The rod motion was synchronously imitated by the motion surrogate platform with a mounted chest plate and was monitored by the clinically used pressure belt system with a sampling rate of 40 Hz (AZ-733V, Anzai Medical Co., Ltd., Tokyo, Japan).

Using the network time protocol, we ensured that the timing information in the motion log files of the independent pressure belt system was correctly synchronized with the reference clock of the proton machine steering system, which provides the timing information for the machine log files.

2.2.2 | 4DCT

For each motion form and amplitude, a 4DCT of the phantom was acquired using a Siemens SOMATOM Definition AS scanner (Siemens Healthineers, Erlangen, Germany) with our standard clinical protocol (tube voltage: 120 kV, quality reference mAs: 85, CareDose4D, pitch: 0.09, rotation time: 500 ms, collimation: 16 × 0.6 mm). The mid elongation of the tumor model remained at the same position relative to the static phantom part in all scans irrespective of the motion magnitude. For each scan, 12 amplitude-based CT phases were reconstructed (iterative reconstruction kernel Q34f with SAFIRE 3) with 2 mm slice distance and 0.98 mm pixel size. The respective reconstruction amplitudes per phase were selected on the acquired surrogate motion curve in such a way that almost the complete curve is sampled (six inhale phases and six exhale phases) and that none of the raw data bins with a temporal width of 250 ms overlap (cf. Figure S1).

2.2.3 | DIR

The automatic intensity- and structure-based algorithm in the TPS (ANACONDA[30]) was used to generate the deformation vector fields between the different CT phases and the end-exhalation phases with the target in the most cranial position. A sufficient vector field quality in terms of geometrical validity was achieved by using the moving rod as “Focus ROI” and additional contours (namely the tumor model, the three radiopaque markers and further well identifiable structures within the rod insert) as “Controlling ROI”. To investigate how remaining deformation uncertainties may influence the final reconstruction results, a second, ground-truth deformation vector field type was generated via the scripting interface. The shifts of the center of mass coordinates of the aforementioned contours were averaged and considered as the vector field amplitude within the moveable rod for the respective CT phase. Only for the 5 mm peak-to-peak amplitudes, where the motion difference

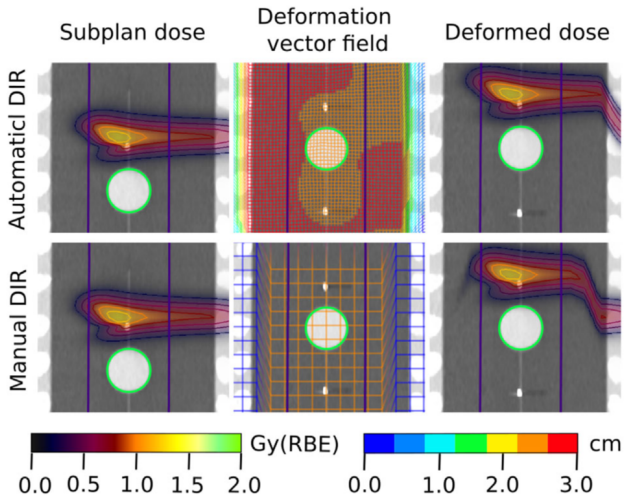

FIGURE 2 Sagittal isocenter plane of a subplan dose distribution at inhalation (left), the deformation vector fields (middle) to the exhalation reference state and resulting deformed dose distribution on the reference computed tomography (CT) (right) according to the automatically generated vector field (top) and manually defined vector field (bottom), both used within the experiments

between adjacent CT phases was much smaller than the CT slice thickness, the vector field amplitudes in the rod were calculated based on the principal knowledge about the phantom motion and the 4DCT reconstruction algorithm. A visualization of the two types of vector fields and their influence on dose deformation are illustrated in Figure 2.

2.2.4 | Treatment plans and delivery

The treatment plans were generated in the TPS RayStation v.7.99.3 (RaySearch Laboratories AB, Stockholm, Sweden) with the clinical beam model for our Proteus PLUS (Ion Beam Applications SA, Louvain-La-Neuve, Belgium) gantry room and considering a constant relative biological effectiveness (RBE) of 1.1. All plans consisted of only one anterior field (0° gantry angle), and the cranio-caudal motion of the target was perpendicular to the incident beam direction and the fast scanning direction of the machine to induce a higher sensitivity to interplay effects in mono-energy layers.[31] We omitted any interplay effect-mitigating strategies such as rescanning, as we aimed to challenge the 4D log file-based dose reconstruction algorithm for reproducing distinctive motion-related dose signatures. For all motion magnitudes, the isocenter was aligned with the center of the spherical tumor model at the respective maximum exhalation phase, which represents the most cranial tumor position within the motion cycle. A range shifter (6.52 cm thick lexane block equal to 7.38 cm water-equivalent thickness) was inserted with an air gap of 2 cm to the phantom surface in all irradiation scenarios.

Two types of treatment plans were generated:

1. Quasi-monoenergetic plans were designed to guarantee distinct interplay patterns on the radiochromic film as the interplay patterns from sequential energy layers of a volumetrically optimized field would most likely countervail each other in the radiochromic film plane. Depending on the individual spot and the current target position, the selected single energy ensured that the protons will either stop shortly before the film (in the target) or stop shortly behind the film while depositing a relevant dose in the film. Thus, even minor errors in log file synchronization or in the spot sorting algorithm during the 4D dose reconstruction will result in distinct differences compared to the dose on the film. For each motion amplitude, 98 spots were placed on 13 lines in a hexagonal grid forming a field size of 5.74 cm × 8.52 cm (Figure 1b) with spot coordinates symmetric to the mid elongation of the respective motion magnitude. The use of high and constant spot weights ensured a clear dose visibility on the radiochromic films and correspond in the static case to a reference/prescription dose of D_p = 4.75 Gy(RBE). As the delivery of the purely monoenergetic field was too fast (6 s) to generate elaborate interplay patterns, we induced an artificial break after each line segment by alternated energy switching between 122 MeV and 123 MeV, and thus, extended the irradiation time considerably to about 47 s. Although these plans contain two energies, we will further refer to them as monoenergetic. For the static case, Figure 1c depicts the distinctive dose distribution in the orthogonal isocenter planes originating from the spot coordinate specific passage through rib material and/or different amount of soft tissue due to the tumor model and the curved phantom geometry.
2. To investigate more realistic treatment plans regarding the spot delivery timing and the shape of the high dose volume, 4D robust plans were optimized for each of the five 4DCTs with sinusoidal motion. The optimization considered a prescription of 2 Gy per fraction to the target region of interest (ROI) defined as the tumor model with 3 mm margin, 3 mm setup uncertainty, 6.3% range uncertainty (corresponding to the clinical safety margin of 3.5% + 2 mm[32,33]), and five of the 12 CT phases including those with extremal elongations.[34,35] The 4D robust plans included on average 439 spots in 13 energy layers with optimized spot weights (cf. Table S1).

In summary, the monoenergetic plans were delivered to the phantom under 10 different conditions (sinusoidal and sin^4 motion, each with five amplitudes) for each of which the inserted radiochromic film was analyzed. The 4D plans were delivered under five different conditions (five peak-to-peak amplitudes of sinusoidal motion). The

delivery characteristics of all plans including beam-on times and average spot delivery times were extracted from the machine log files.

2.3 | Analyses of reconstructed dose distributions

2.3.1 | Comparison of 2D measured and reconstructed dose distributions

For the comparison with film dose measurements, we repeated each 4D log file-based dose reconstruction from monoenergetic field irradiations with four different settings, namely with both sets of vector fields (from automatic or manual DIR) and applying either a fine dose grid resolution of 1 mm or the clinically used 3 mm resolution. The radiochromic films were scanned 3–6 days after irradiation with a flat-bed document scanner (Expression 11000L, EPSON America, Long Beach, CA, USA) with a resolution of 300 dpi (11.81 dpmm). The optical density in the red channel of all pixels except those close to the cutting edges was analyzed with an in-house developed software and converted to dose. However, the film dose response curve depends on the linear energy transfer.[36,37] The films imaged the characteristic proton dose patterns close to/within the Bragg peak depth (compare transversal and sagittal slice in Figure 1c) and as the actual depth changes locally just to a minor extent with the unpredictable interplay, we added a global quenching correction of 20%[38–40] in all measurements. Corresponding 2D dose distributions at isocenter depth were extracted from the 4D log file-based dose reconstructions via the scripting interface in the TPS. Measured and reconstructed physical doses were compared by a 2D γ-analysis with 3 mm distance to agreement and 3% global dose difference criterion in OmniPro I'mRT (v1.7b, IBA Dosimetry, Schwarzenbruck, Germany) after the alignment of the film dose distribution based on the position of the three radiopaque markers and the conversion of both dose grids to a 1 mm resolution. A constant area of 12.5 cm $\times$ 4.8 cm was considered for y-pass rate determination and a low-dose threshold of 10% was applied.

For statistical evaluation, a model based on generalized estimating equations with linear link function was applied. The γ-pass rates (dependent variable) were transformed with ln(100 - γ-pass rate [%]) to achieve an approximate normal distribution. Independent factors were motion amplitude, motion wave form, dose grid resolution, and used DIR. An index (ranging from 1 to 40) was assigned to each reconstructed dose distribution with different parameters and considered as the repeated subject variable. A robust estimate was used for the covariance matrix and the working correlation matrix was assumed to be exchangeable. Analysis was performed in SPSS Statistics (v27, IBM Deutschland GmbH, Ehningen, Germany). Resulting p values were interpreted as statistically significant for $p < 0.05$ and as trending toward significance for $0.05 \leq p < 0.1$.

2.3.2 | Sensitivity to asynchronized log files

The effect of temporal asynchronies between the motion log files and the machine log files on the reconstructed dose distributions was investigated for all measurements with sinusoidal motion by artificially shifting the time stamps of the motion log files by $\pm$1 ms, $\pm$5 ms, $\pm$25 ms, $\pm$50 ms, or $\pm$250 ms. A 3 mm dose grid resolution and the manually defined vector fields were used for the reconstructions. The retrieved dose distributions were compared to the nominal ones with synchronized log files as follows: (1) a global 3D γ-analysis (1 mm, 1%) with a low-dose threshold of 10% was performed in 3D Slicer.[41] (2) The distribution of the absolute dose differences relative to the prescribed dose ($|\Delta D|$) was calculated from the dose distributions of nominal and shifted log files as $|\Delta D| = |(D_{shift} - D_{nom})/D_p|$ and its dose volume histogram parameters D_{1ml}, $V_{1\%}$, and $V_{5\%}$ were extracted for the phantom's external (cf. Figure S3 for illustration purpose). These parameters indicate the near maximum absolute dose difference and the volumes with absolute dose differences of more than 1% and 5% of the prescribed dose, respectively.

3 | RESULTS

3.1 | Beam delivery characteristics

All plans were delivered with the clinical machine and records were kept in the machine log files with subspot resolution by a sampling rate of 4 kHz. Excluding the energy switching times, the mean and standard deviation of the delivery time for the 98 spots in the monoenergetic fields was 3.4 s $\pm$ 0.6 s, corresponding to 34.3 ms $\pm$ 5.6 ms per spot (including spot switching time). The large standard deviation is rather related to updated machine configurations applied by the vendor between experiment sessions than to the day-to-day variability of the treatment machine. The total beam-on time of the 4D optimized plans ranged between 3.1 s and 8.9 s, which implies an average delivery time per spot of about 13.5 ms $\pm$ 4.9 ms. Detailed characteristics per plan are listed in Supporting Information 2.

3.2 | Comparison of 2D measured and reconstructed dose distributions

The measured and reconstructed dose distributions with their characteristic interplay patterns for the monoenergetic fields on the coronal isocenter plane are in good

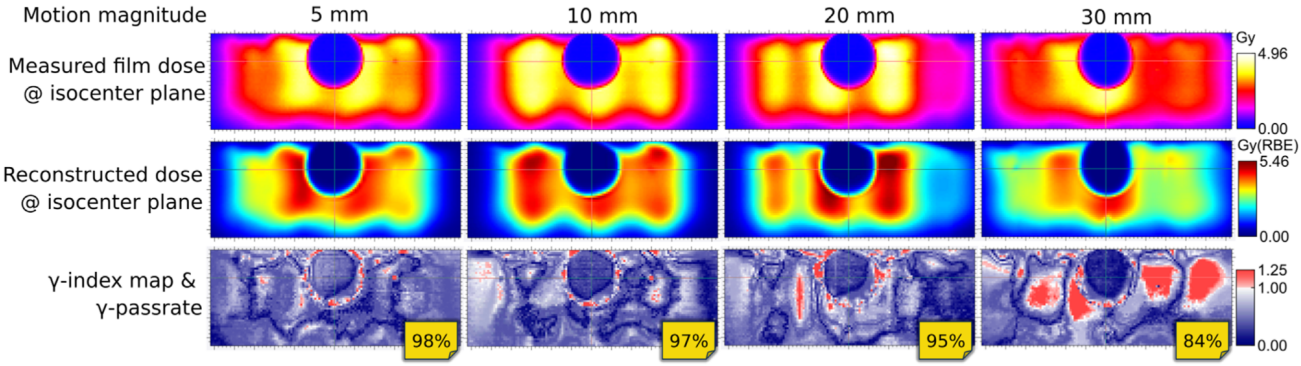

FIGURE 3 Examples of the visual comparison between measured film doses (top) and reconstructed doses (middle, exemplary reconstruction with 1 mm dose grid resolution and manual deformable image registration [DIR]) at the isocenter plane for different peak-to-peak motion amplitudes and sinusoidal motion. The results of the 2D γ-analysis (3 mm, 3%) as well as the γ-pass rates are shown in the bottom row

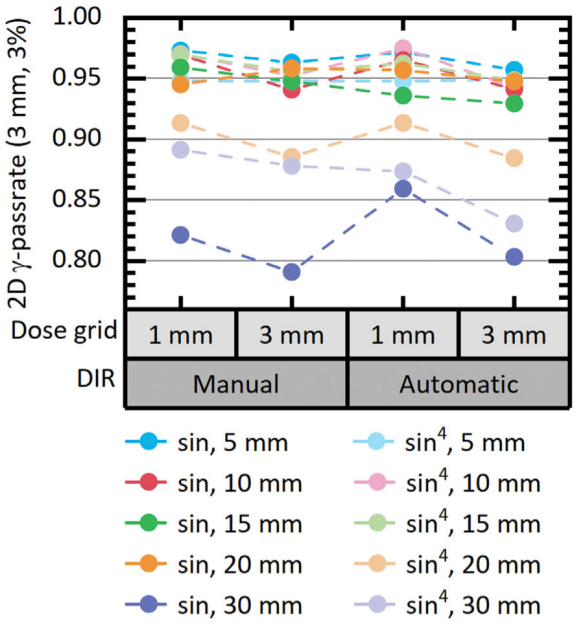

FIGURE 4 Pass rates of the 2D γ-analysis with (3 mm, 3%) criterion between the measured film dose and the reconstructed dose distributions at isocenter plane for different motion amplitudes, wave forms, dose grid resolutions, and deformable image registrations (DIR)

visual agreement (Figure 3). The influence of motion amplitude and wave form, dose grid resolution and DIR on the resulting γ-pass rates was quantified (Figure 4). The motion amplitude had a significant influence on the γ-pass rates ($p < 0.001$) with a negative correlation. For motion amplitudes ≤15 mm, the γ-pass rates were above 95% for most cases. There was a clear decline in the γ-pass rates for motion amplitudes ≥20 mm. Significantly higher γ-pass rates were achieved when using the 1 mm dose grid resolution ($p < 0.001$). There was no significant difference between the used DIRs, but there was a trend toward higher γ-pass rates for the manually defined vector field ($p = 0.073$). The motion wave form (*sin* vs. sin^4) did not significantly influence the results of the γ-analysis ($p = 0.646$).

3.3 | Sensitivity to asynchronized log files

Due to the asynchronized log files, single PBS spots are assigned to subplans of the adjacent 4DCT phases. The exact number of erroneously sorted spots depends on the individual interplay of motion and beam delivery, the actual breathing pattern, the motion period T and number of CT phases N. As a rule of thumb, the fraction of missorted spots for a small time shift ΔT between both log files will be about $N \bullet \Delta T/T$. For the investigated asynchronies, spots were falsely assigned solely to the adjacent 4DCT phases.

The influence of artificially inserted offsets between machine and motion log files on the reconstruction result was quantified for the different investigated motion amplitudes and treatment plan types (Figure 5). All doses were reconstructed using the manually defined deformation vector field as it showed beneficial results in the previous evaluation and higher plausibility across the whole phantom geometry (cf. Figure S4). The monoenergetic fields and the 4D robustly optimized plans showed a similar behavior. The γ-pass rates for the global 3D γ-analyses decreased with increasing asynchronies and motion amplitudes (Figure 5a). The γ-pass rate remained above 95% for the 5 mm motion magnitude with all investigated asynchronies, and for higher motion amplitudes with time offsets of up to 5 ms. Regarding the distribution of absolute dose differences within the whole phantom geometry, there was a clear increase in D_{1ml} for higher asynchronies and motion amplitudes (Figure 5b). D_{1ml} remains below 5% both for small motions of 5 mm regardless of the asynchrony and for larger motion amplitudes with asynchronies of maximal 5 ms. A similar behavior was found for the volumes of maximal absolute dose differences $V_{1\%}$ and $V_{5\%}$. The more sensitive parameter $V_{1\%}$ shows a steady increase for higher asynchronies and motion amplitudes (Figure 5c). The absolute dose deviations of more than 5% remained neglectable for asynchronies ≤25 ms

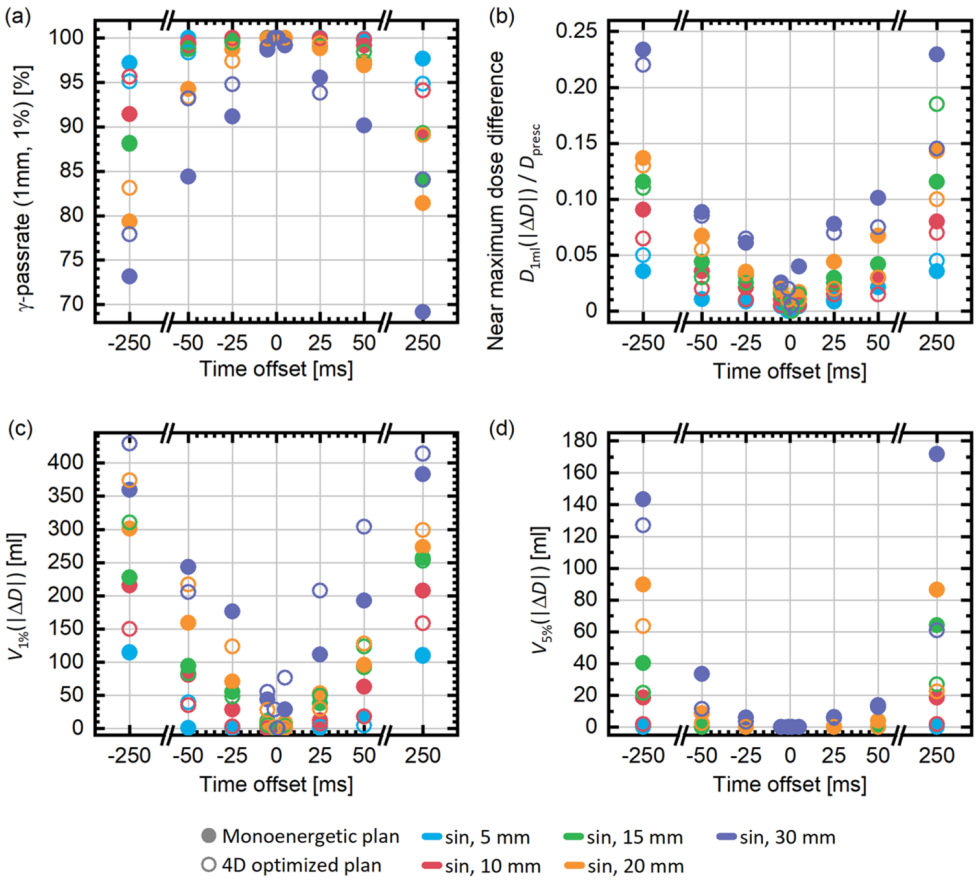

FIGURE 5 Comparison between 4D log file-based dose reconstructions with synchronized and asynchronized machine and motion log files by (a) pass rates of 3D γ-analyses with (1 mm, 1%) criterion and 10% dose threshold and (b–d) dose volume histogram parameters of the absolute dose difference distribution in the phantom external indicating the near maximum dose difference relative to the prescribed dose (b) and the volumes with absolute dose differences of more than 1% (c) and 5% (d) of the prescribed dose, respectively. Results are shown for the monoenergetic (full circle) and the 4D optimized plans (empty circle) with sinusoidal wave form and different amplitudes (indicated by different colors)

(below 7 ml for 30 mm motion magnitude; 0 ml otherwise), but showed a steep increase for combinations of bigger asynchronies and large amplitudes (Figure 5d). Overall, there is a clear increase in the maximum absolute dose differences as well as in the volumes of relevant dose deviations for larger asynchronies and motion amplitude.

4 | DISCUSSION

A 4D log file-based proton dose calculation is a valuable tool for documenting the actual dose deposition when treating intrafractionally moving targets. As 4DCT images of a patient are the basis for the dose calculations, such an algorithm needs to be in accordance with the 4DCT reconstruction method to yield accurate results. Before applying the 4D log file-based proton dose calculation in clinical routine use, it is essential to verify its correct performance and sensitivity against input parameter variations by dedicated test scenarios, as the reconstruction results might influence the clinician's treatment decision, either in the phase of plan selection (when analyses are performed during pretreatment simulations) or regarding a plan adaptation (when used as dose tracking tool during the treatment course). Within this study, we have benchmarked our 4D log file-based dose reconstruction algorithm by comprehensive measurements with a dynamic phantom under well-defined conditions generating interplay effects from variable amounts of lung, soft and bony tissue surrogates in the beam paths. Specifically, the influence of different amplitudes of regular motion patterns and reconstruction parameters on the reconstruction results was analyzed for an algorithm dedicated to consider the relative amplitude-sorted 4DCTs used at the UPTD.

The characteristic interplay patterns seen at the isocenter plane of the reconstructed dose distributions in the phantom matched with the measured film doses for the different motion amplitudes and wave forms. Two-dimensional γ-analysis showed strong agreement between the measured and the reconstructed doses with γ-pass rates >95% for motion amplitudes of up to 15 mm. There was a clear decline in the γ-pass rates for

higher motion amplitudes, potentially related to the discretization in the 4DCT and the residual motion in the single CT phases. While the general agreement was significantly improved by a higher dose grid resolution, the minor influence of the DIR used was not significant, most likely due to the high similarities of the DIRs in the area imaged by the radiochromic film inside the moving rod (Figure S4). We showed that the accuracy of the reconstructed dose distribution does not depend on the chosen symmetric (*sin*) or asymmetric (sin^4) motion pattern.

The sensitivity of the 4D log file-based dose reconstruction against asynchronies between the machine and motion log files were investigated for artificial offsets ranging from 1 ms to 250 ms, that is between the order of magnitude of the machine log file time resolution and the 4DCT phase duration, respectively. The 3D γ-pass rates remained above 95% for offsets of up to 5 ms, even for large motion amplitudes and independent on the used plan type (monoenergetic or 4D robustly optimized). This indicates that the algorithm is robust enough against potentially remaining clock offsets,[42] which we have observed in the local network of our clinical environment to be within $\pm$5 ms (smaller than the time resolution in the motion log files), and that it yields accurate results for the applied dose even for larger target motions. As such, the findings of this work were essential for the clinical implementation of fraction-wise 4D log file-based dose reconstruction, which can be used to monitor the applied dose over the course of the treatment in the presence of breathing-induced target motion when using PBS proton therapy.

In this study, we used 12 phases in the 4DCT phase reconstruction as opposed to the commonly clinically used 8–10 phases.[21,43] We decided for a higher than usual number of phases for two reasons: the higher number of non-overlapping reconstructed phases leads to a better sampling of the motion curve data and therefore to smaller geometrical differences between adjacent 4DCT phases. This improves the representation of the continuous target motion and the results of the 4D log file-based dose reconstruction as a more continuous reflection of the actual dose delivery. At the same time, asynchronies between the log files have a larger influence on the reconstruction results when using more 4DCT phases since more spots are assigned to other, possibly false, subplans. These two points imply that the results of the dose reconstruction under clinical conditions are expected to be slightly less accurate in the spot sorting due to a higher level of discretization between each phase, but also less prone to log file asynchronies.

Further influencing factors on the accuracy of the dose reconstruction in patient treatment include irregularity of breathing and limited correlation between the external breathing motion and the internal patient anatomy motion estimated by a 4DCT.[44–46] Using the same device for motion monitoring during 4DCT acquisition as during treatment irradiation improves the comparability of the measured breathing curve data. Still, realistic patient breathing patterns may show day-to-day variations in frequency, absolute amplitude and shape, which influences the accuracy of the represented patient anatomy in the 4DCT images. It is therefore of great importance that interfractional changes of the patient's breathing pattern and anatomy are monitored during the entire treatment course,[47] for example by means of weekly 4DCT or even daily cone-beam CT. Breathing guidance strategies during 4DCT acquisition as well as during irradiation can also be applied to improve image quality and breathing regularity.[48,49]

As we aimed to test the accuracy of the dose reconstruction algorithm under extreme conditions, the investigated treatment plans were all limited to one beam perpendicular to the radiochromic film to enhance possible interplay effects. We did not apply any form of motion mitigation and used high MU per spot to create characteristic interplay patterns on the irradiated films. Clinical patient treatment plans would contain more beams from different angles and possibly higher spot numbers with lower MU per spot than the examined plans (or even rescanning), which should reduce the magnitude of interplay effects per fraction.

We performed just one measurement for each motion pattern per scenario. Thus, due to the stochastic nature of the interplay effect, the presented results are snap shots, giving an estimate of the 4D dose reconstruction quality. They should therefore not be interpreted as definite values. Repeat measurements may yield a range of possible dose distortions. However, to ensure that the results of repeat measurements would represent a full range of possible dose distortions with respect to the starting phase, the experiments would require a stable beam delivery timing (cf. Supporting Information 4) and a synchronization of the irradiation start with the breathing cycle phase of the tumor motion, which was not possible with our setup.

When extracting the reconstructed 2D dose distribution from the TPS, the pixel size of about 1 mm in the coronal direction of the CT limits the accuracy in determining the CT slice of the film. In addition to that, the resolution of the scanned film doses is considerably higher than even the fine dose grid resolution of 1 mm in the TPS. Therefore, both resolutions were scaled to the same size for the 2D γ-analysis.

Imaging artifacts are a further limiting factor for the accuracy of the 4D dose reconstruction.[50] Especially for larger motion amplitudes, an increase of motion artifacts in the 4DCT phases was visible, which could only be improved by a faster rotation time of the X-ray tube.

In general, the accuracy of a DIR influences the results of the 4D dose reconstruction.[51,52] By establishing a ground truth with the manually set deformation vector fields based on the knowledge of the phantom geometry, we were able to exclude the DIR uncertainty

from the performance analysis of the dose reconstruction algorithm. As the pure gray level-based automatic DIR is by default not suited for the sliding rod motion in the lung of the phantom (cf. Figure S5), we used focus and controlling ROIs within the phantom to guide the deformation algorithm into creating satisfactory vector deformation fields. Thus, we could confirm with our experiments an accurate dose reconstruction (for motions of up to 15 mm) as long as there are sufficiently correct deformation vector fields. As the ground truth of the deformation inside the patient is usually unknown, it is of importance to check the deformation vector fields for plausibility and to modify the generation of the vector fields if needed.

Overall, the 4D log file-based dose reconstruction yields satisfactory results even for high motion amplitudes and in the presence of minor temporal asynchronies between motion and machine log files. Meanwhile, we have clinically implemented and optimized a workflow of fraction-wise 4D dose reconstruction as an additional quality assurance to monitor the applied dose distribution in the patients alongside treatment. This was a prerequisite in our clinic to start PBS treatment of patients with breathing-induced target motion in the thoracic region. The acquired clinical data can be used to further analyze the influence of patient and treatment parameters and to improve treatment robustness of moving targets in the future.

5 | CONCLUSIONS

We have successfully implemented a 4D log file-based proton dose reconstruction algorithm accounting for amplitude-sorted 4DCTs and have experimentally validated that sufficiently correct dose distributions are obtained for motion magnitudes $\leq$15 mm when using our standard clinically applied dose grid resolution and DIR algorithm. Robustness against temporal asynchronies between motion and machine log files was confirmed for latencies below the time resolution of the motion monitoring system. Particular attention must be paid to the synchronization of the two log file generating systems, especially for large motion amplitudes. After the experimental characterization of the 4D log file-based dose reconstruction, we have started its routine application for PBS proton therapy of patients with thoracic malignancies and breathing-induced target motion.

ACKNOWLEDGMENTS

The authors thank Andreas Schumann who has supported together with Uwe Just the synchronization between both log file-generating systems and assisted in the machine log file retrieval and post-processing; Elke Beyreuther for her help regarding the radiochromic film analysis; Maria Tschiche, Stefan Menkel, and Anne-Kristin Dietert for the discussions and help with 4DCT scans and experiment preparations; and Bradley Oborn for proof-reading the manuscript.

Open access funding enabled and organized by Projekt DEAL.

CONFLICTS OF INTEREST

OncoRay has an institutional research agreement with IBA, but there was no influence on the authors during this study, neither in terms of the study design, data analysis, and interpretation nor the writing of the manuscript.

FUNDING INFORMATION

The authors received no funding for this work.

DATA AVAILABILITY STATEMENT

The datasets generated and analyzed during the current study are available from the corresponding author on reasonable request.

REFERENCES

1. Phillips MH, Pedroni E, Blattmann H, Boehringer T, Coray A, Scheib S. Effects of respiratory motion on dose uniformity with a charged particle scanning method. *Phys Med Biol*. 1992;37(1):223-234. https://doi.org/10.1088/0031-9155/37/1/016
2. Bert C, Grözinger SO, Rietzel E. Quantification of interplay effects of scanned particle beams and moving targets. *Phys Med Biol*. 2008;53(9):2253-2265. https://doi.org/10.1088/0031-9155/53/9/003
3. Dowdell S, Grassberger C, Sharp GC, Paganetti H. Interplay effects in proton scanning for lung: a 4D Monte Carlo study assessing the impact of tumor and beam delivery parameters. *Phys Med Biol*. 2013;58(12):4137-4156. https://doi.org/10.1088/0031-9155/58/12/4137
4. Kraus KM, Heath E, Oelfke U. Dosimetric consequences of tumour motion due to respiration for a scanned proton beam. *Phys Med Biol*. 2011;56(20):6563-6581. https://doi.org/10.1088/0031-9155/56/20/003
5. Grassberger C, Daartz J, Dowdell S, Ruggieri T, Sharp G, Paganetti H. Quantification of proton dose calculation accuracy in the lung. *Int J Radiat Oncol Biol Phys*. 2014;89(2):424-430. https://doi.org/10.1016/j.ijrobp.2014.02.023
6. Seco J, Panahandeh HR, Westover K, Adams J, Willers H. Treatment of non-small cell lung cancer patients with proton beam-based stereotactic body radiotherapy: dosimetric comparison with photon plans highlights importance of range uncertainty. *Int J Radiat Oncol Biol Phys*. 2012;83(1):354-361. https://doi.org/10.1016/j.ijrobp.2011.05.062
7. Schätti A, Zakova M, Meer D, Lomax AJ. Experimental verification of motion mitigation of discrete proton spot scanning by re-scanning. *Phys Med Biol*. 2013;58(23):8555-8572. https://doi.org/10.1088/0031-9155/58/23/8555
8. Grassberger C, Dowdell S, Sharp G, Paganetti H. Motion mitigation for lung cancer patients treated with active scanning proton therapy. *Med Phys*. 2015;42(5):2462-2469. https://doi.org/10.1118/1.4916662
9. Schätti A, Zakova M, Meer D, Lomax AJ. The effectiveness of combined gating and re-scanning for treating mobile targets with proton spot scanning. An experimental and simulation-based investigation. *Phys Med Biol*. 2014;59(14):3813-3828. https://doi.org/10.1088/0031-9155/59/14/3813
10. Furukawa T, Inaniwa T, Sato S, et al. Moving target irradiation with fast rescanning and gating in particle therapy. *Med Phys*. 2010;37(9):4874-4879. https://doi.org/10.1118/1.3481512

11. Lu HM, Brett R, Sharp G, et al. The development and commissioning of a respiratory-gated treatment system for proton therapy. *IFMBE Proc*. 2007;14(1):2215-2218. https://doi.org/10.1007/978-3-540-36841-0_559
12. Kanehira T, Matsuura T, Takao S, et al. Impact of real-time image gating on spot scanning proton therapy for lung tumors: a simulation study. *Int J Radiat Oncol Biol Phys*. 2017;97(1):173-181. https://doi.org/10.1016/j.ijrobp.2016.09.027
13. Engelsman M, Rietzel E, Kooy HM. Four-dimensional proton treatment planning for lung tumors. *Int J Radiat Oncol Biol Phys*. 2006;64(5):1589-1595. https://doi.org/10.1016/j.ijrobp.2005.12.026
14. Liu W, Schild SE, Chang JY, et al. Exploratory study of 4D versus 3D robust optimization in intensity modulated proton therapy for lung cancer. *Int J Radiat Oncol Biol Phys*. 2016;95(1):523-533. https://doi.org/10.1016/j.ijrobp.2015.11.002
15. Heinzerling JH, Anderson JF, Papiez L, et al. Four-dimensional computed tomography scan analysis of tumor and organ motion at varying levels of abdominal compression during stereotactic treatment of lung and liver. *Int J Radiat Oncol Biol Phys*. 2008;70(5):1571-1578. https://doi.org/10.1016/j.ijrobp.2007.12.023
16. Mampuya WA, Nakamura M, Matsuo Y, et al. Interfraction variation in lung tumor position with abdominal compression during stereotactic body radiotherapy. *Med Phys*. 2013;40(9):091718/1-7. https://doi.org/10.1118/1.4819940
17. Ribeiro CO, Visser S, Korevaar EW, et al. Towards the clinical implementation of intensity-modulated proton therapy for thoracic indications with moderate motion: robust optimised plan evaluation by means of patient and machine specific information. *Radiother Oncol*. 2021;157:210-218. https://doi.org/10.1016/j.radonc.2021.01.014
18. Ribeiro CO, Meijers A, Korevaar EW, et al. Comprehensive 4D robustness evaluation for pencil beam scanned proton plans. *Radiother Oncol*. 2019;136:185-189. https://doi.org/10.1016/j.radonc.2019.03.037
19. Fracchiolla F, Dionisi F, Giacomelli I, et al. Implementation of proton therapy treatments with pencil beam scanning of targets with limited intrafraction motion. *Phys Med*. 2019;57:215-220. https://doi.org/10.1016/j.ejmp.2019.01.007
20. Juhler Nøttrup T, Korreman SS, Pedersen AN, et al. Intra- and interfraction breathing variations during curative radiotherapy for lung cancer. *Radiother Oncol*. 2007;84(1):40-48. https://doi.org/10.1016/j.radonc.2007.05.026
21. den Otter LA, Anakotta RM, Weessies M, et al. Investigation of inter-fraction target motion variations in the context of pencil beam scanned proton therapy in non-small cell lung cancer patients. *Med Phys*. 2020;47(9):3835-3844. https://doi.org/10.1002/mp.14345
22. Dhont J, Vandemeulebroucke J, Burghelea M, et al. The long- and short-term variability of breathing induced tumor motion in lung and liver over the course of a radiotherapy treatment. *Radiother Oncol*. 2018;126(2):339-346. https://doi.org/10.1016/j.radonc.2017.09.001
23. Richter D, Saito N, Chaudhri N, et al. Four-dimensional patient dose reconstruction for scanned ion beam therapy of moving liver tumors. *Int J Radiat Oncol Biol Phys*. 2014;89(1):175-181. https://doi.org/10.1016/j.ijrobp.2014.01.043
24. Krieger M, Klimpki G, Fattori G, et al. Experimental validation of a deforming grid 4D dose calculation for PBS proton therapy. *Phys Med Biol*. 2018;63(5):055005 (11pp). https://doi.org/10.1088/1361-6560/aaad1e
25. Pfeiler T, Bäumer C, Engwall E, Geismar D, Spaan B, Timmermann B. Experimental validation of a 4D dose calculation routine for pencil beam scanning proton therapy. *Z Med Phys*. 2018;28(2):121-133. https://doi.org/10.1016/j.zemedi.2017.07.005
26. Kostiukhina N, Palmans H, Stock M, Knopf A, Georg D, Knäusl B. Time-resolved dosimetry for validation of 4D dose calculation in PBS proton therapy. *Phys Med Biol*. 2020;65(12):125015 (13pp). https://doi.org/10.1088/1361-6560/ab8d79
27. Meijers A, Jakobi A, Stützer K, et al. Log file-based dose reconstruction and accumulation for 4D adaptive pencil beam scanned proton therapy in a clinical treatment planning system: implementation and proof-of-concept. *Med Phys*. 2019;46(3):1140-1149. https://doi.org/10.1002/mp.13371
28. Abdelnour AF, Nehmeh SA, Pan T, et al. Phase and amplitude binning for 4D-CT imaging. *Phys Med Biol*. 2007;52:3515-3529. https://doi.org/10.1088/0031-9155/52/12/012
29. Li H, Noel C, Garcia-Ramirez J, et al. Clinical evaluations of an amplitude-based binning algorithm for 4DCT reconstruction in radiation therapy. *Med Phys*. 2012;39(2):922-932. https://doi.org/10.1118/1.3679015
30. Weistrand O, Svensson S. The ANACONDA algorithm for deformable image registration in radiotherapy. *Med Phys*. 2015;42(1):40-53. https://doi.org/10.1118/1.4894702
31. Fattori G, Klimpki G, Hrbacek J, et al. The dependence of interplay effects on the field scan direction in PBS proton therapy. *Phys Med Biol*. 2019;64(9):095005 (12pp). https://doi.org/10.1088/1361-6560/ab1150
32. Taasti VT, Bäumer C, Dahlgren CV, et al. Inter-centre variability of CT-based stopping-power prediction in particle therapy: survey-based evaluation. *Phys Imaging Radiat Oncol*. 2018;6(April):25-30. https://doi.org/10.1016/j.phro.2018.04.006
33. Paganetti H. Range uncertainties in proton therapy and the role of Monte Carlo simulations. *Phys Med Biol*. 2012;57(11):R99-R117. https://doi.org/10.1088/0031-9155/57/11/R99
34. Feng H, Shan J, Ashman JB, et al. Technical note: 4D robust optimization in small spot intensity-modulated proton therapy (IMPT) for distal esophageal carcinoma. *Med Phys*. 2021;48(8):4636-4647. https://doi.org/10.1002/mp.15003
35. Cummings D, Tang S, Ichter W, et al. Four-dimensional plan optimization for the treatment of lung tumors using pencil-beam scanning proton radiotherapy. *Cureus*. 2018;10(8):e3192. https://doi.org/10.7759/cureus.3192
36. Battaglia MC, Schardt D, Espino JM, et al. Dosimetric response of radiochromic films to protons of low energies in the Bragg peak region. *Phys Rev Accel Beams*. 2016;19(6):064701/1-7. https://doi.org/10.1103/PhysRevAccelBeams.19.064701
37. Castriconi R, Ciocca M, Mirandola A, et al. Dose-response of EBT3 radiochromic films to proton and carbon ion clinical beams. *Phys Med Biol*. 2017;62(2):377-393. https://doi.org/10.1088/1361-6560/aa5078
38. Anderson SE, Grams MP, Wan Chan Tseung H, Furutani KM, Beltran CJ. A linear relationship for the LET-dependence of Gafchromic EBT3 film in spot-scanning proton therapy. *Phys Med Biol*. 2019;64(5):055015 (8pp). https://doi.org/10.1088/1361-6560/ab0114
39. Zhao L, Das IJ. Gafchromic EBT film dosimetry in proton beams. *Phys Med Biol*. 2010;55(10):N291-N301. https://doi.org/10.1088/0031-9155/55/10/N04
40. Vadrucci M, Esposito G, Ronsivalle C, et al. Calibration of GafChromic EBT3 for absorbed dose measurements in 5 MeV proton beam and 60Co γ-rays. *Med Phys*. 2015;42(8):4678-4684. https://doi.org/10.1118/1.4926558
41. Pinter C, Lasso A, Wang A, Jaffray D, Fichtinger G. SlicerRT: radiation therapy research toolkit for 3D slicer. *Med Phys*. 2012;39(10):6332-6338. https://doi.org/10.1118/1.4754659
42. Wang L, Fernandez J, Burgett J, Conners RW, Liu Y. An evaluation of network time protocol for clock synchronization in wide area measurements. In: *IEEE Power and Energy Society 2008 General Meeting – Conversion and Delivery of Electrical Energy in the 21st Century (PES)*. IEEE; 2008:1-5. https://doi.org/10.1109/PES.2008.4596234

43. Lambrecht M, Sonke JJ, Nestle U, et al. Quality assurance of four-dimensional computed tomography in a multicentre trial of stereotactic body radiotherapy of centrally located lung tumours. *Phys Imaging Radiat Oncol*. 2018;8:57-62. https://doi.org/10.1016/j.phro.2018.10.003
44. Knybel L, Cvek J, Molenda L, Stieberova N, Feltl D. Analysis of lung tumor motion in a large sample: patterns and factors influencing precise delineation of internal target volume. *Int J Radiat Oncol Biol Phys*. 2016;96(4):751-758. https://doi.org/10.1016/j.ijrobp.2016.08.008
45. Hoisak JDP, Sixel KE, Tirona R, Cheung PCF, Pignol JP. Correlation of lung tumor motion with external surrogate indicators of respiration. *Int J Radiat Oncol Biol Phys*. 2004;60(4):1298-1306. https://doi.org/10.1016/j.ijrobp.2004.07.681
46. Ionascu D, Jiang SB, Nishioka S, Shirato H, Berbeco RI. Internal-external correlation investigations of respiratory induced motion of lung tumors. *Med Phys*. 2007;34(10):3893-3903. https://doi.org/10.1118/1.2779941
47. Meijers A, Knopf AC, Crijns APG, et al. Evaluation of interplay and organ motion effects by means of 4D dose reconstruction and accumulation. *Radiother Oncol*. 2020;150:268-274. https://doi.org/10.1016/j.radonc.2020.07.055
48. Pollock S, Keall R, Keall P. Breathing guidance in radiation oncology and radiology: a systematic review of patient and healthy volunteer studies. *Med Phys*. 2015;42(9):5490-5509. https://doi.org/10.1118/1.4928488
49. Oh SA, Yea JW, Kim SK, Park JW. Optimal gating window for respiratory-gated radiotherapy with real-time position management and respiration guiding system for liver cancer treatment. *Sci Rep*. 2019;9(1):1-6. https://doi.org/10.1038/s41598-019-40858-2
50. Zhang Y, Huth I, Weber DC, Lomax AJ. Dosimetric uncertainties as a result of temporal resolution in 4D dose calculations for PBS proton therapy. *Phys Med Biol*. 2019;64(12):125005 (10pp). https://doi.org/10.1088/1361-6560/ab1d6f
51. Ribeiro CO, Knopf A, Langendijk JA, Weber DC, Lomax AJ, Zhang Y. Assessment of dosimetric errors induced by deformable image registration methods in 4D pencil beam scanned proton treatment planning for liver tumours. *Radiother Oncol*. 2018;128(1):174-181. https://doi.org/10.1016/j.radonc.2018.03.001
52. Nenoff L, Ribeiro CO, Matter M, et al. Deformable image registration uncertainty for inter-fractional dose accumulation of lung cancer proton therapy. *Radiother Oncol*. 2020;147:178-185. https://doi.org/10.1016/j.radonc.2020.04.046

SUPPORTING INFORMATION

Additional supporting information may be found in the online version of the article at the publisher's website.

How to cite this article: Spautz S, Jakobi A, Meijers A, et al. Experimental validation of 4D log file-based proton dose reconstruction for interplay assessment considering amplitude-sorted 4DCTs. *Med Phys*. 2022;49:3538–3549. https://doi.org/10.1002/mp.15625